# Neutron and x-ray scattering studies of field-cooled ordering in the three-dimensional random-field Ising model

Q. Feng, Q. J. Harris, and R. J. Birgeneau
*Department of Physics, Massachusetts Institute of Technology, Cambridge, Massachusetts 02139*

J. P. Hill
*Department of Physics, Brookhaven National Laboratory, Upton, New York 11973*

(Received 24 July 1996)

We report a magnetic neutron and x-ray scattering study of the correlation length and order parameter of the random-field Ising magnets $Fe_{0.5}Zn_{0.5}F_2$ and $Mn_{0.45}Zn_{0.55}F_2$ on field cooling. Fitting the inverse correlation length, $\kappa$, measured above the metastability temperature, $T_M(H)$ in $Fe_{0.5}Zn_{0.5}F_2$, at $H=5$ and 6 T to a power law yields the exponent $\nu=1.5\pm0.3$ together with the equilibrium transition temperatures, $T_N(H)$, which are found to be well below $T_M(H)$. We also estimate $\gamma=2.6\pm0.5$ and $\overline{\gamma}=5.7\pm1$ for the connected susceptibility, $\chi$, and the disconnected susceptibility, $\chi_{\rm dis}$, exponents, respectively. The x-ray data reveal a long range ordered component coexisting with short range magnetic order in the field-cooled state, for weak random fields in both samples. The nucleation of the long range order occurs below $T_M(H)$. The intensity of the long range order component decreases with increasing field. [S0163-1829(97)03401-2]

## I. INTRODUCTION

Despite over two decades of theoretical and experimental effort, our understanding of both the equilibrium and nonequilibrium properties of the random-field Ising model (RFIM) remains incomplete. Theoretically, the lower critical dimension in equilibrium is now generally accepted to be 2. However, there has been only limited progress[1–3] on the basic questions of the order of the transition and the values of the critical exponents. Most experimental information has been obtained from various diluted antiferromagnets in an applied field (DAFF).[4] However, experimental results in three dimensions (3D) are difficult to interpret due to the presence of nonequilibrium effects. These result in, for example, the large hysteresis between the zero-field-cooling (ZFC) and the field-cooling (FC) experimental protocols. In zero-field cooling, a diluted antiferromagnet is first cooled through the zero-field Néel transition, which is characterized by random exchange critical behavior. The resultant long range magnetic order (LRO) is largely preserved when the external field is subsequently turned on and gradually diminishes as the sample is then heated into the paramagnetic phase, passing through a rounded ZFC transition. When cooled in a field, the sample falls out of equilibrium, at $T_M(H)$, and develops a metastable short range ordered (SRO) domain state without ever achieving long range order. This type of hysteresis has been observed directly by neutron and magnetic x-ray scattering[5–12] and indirectly by many techniques including uniform magnetization,[13,14] Faraday rotation,[15] linear magnetic birefringence,[16] and thermal expansion.[17] The disparate behavior of the ZFC and the FC protocols has also been observed in Monte Carlo simulations.[18–22] In the preceding paper, Ref. 23, which should be viewed as the companion paper to the present study, the ZFC transition was investigated and discussed in detail. In the present paper, we focus on the ordering obtained on field cooling, as revealed by x-ray and neutron scattering studies of two diluted antiferromagnets, $Mn_{0.45}Zn_{0.55}F_2$ and $Fe_{0.5}Zn_{0.5}F_2$.

The hysteretic effects and other nonequilibrium behaviors are attributed to the unusual activated random-field dynamics, proposed by Villain[24] and Fisher.[25] The static random-field fluctuations dominate the dynamic behavior and result in pathologically slow relaxations. In practice, this makes it impossible to observe the equilibrium random-field Ising transition in three dimensions on finite time scales. Thus the predictions for the order of the transition and the values of the critical exponents, and even the lower critical dimension, remain largely untested experimentally. Note that the ZFC state, though possessing long range order, is in fact also a metastable state and that the ZFC transition is a superheated transition that occurs at a temperature higher than the presumed equilibrium random-field transition temperature. Because the ZFC state has been assumed to be close to the equilibrium long range ordered ground state of the 3D RFIM and because the transition at low fields displays apparently sharp and distinctive features in observable quantities, it has been studied intensively by many experimental methods. The interpretation of the ZFC transition behavior has remained controversial, and is addressed in detail in the companion paper, Ref. 23.

Experiments in the field-cooled state have largely focused on the scaling of domain size with random-field strength[5,6] and the time dependent behavior.[27,15,28,13] The field-cooled transition, which results in a nonequilibrium domain state and is largely featureless, has not been studied as much as the ZFC transition. However, there exists a well defined metastability temperature, $T_M(H)$, above which no hysteresis is observed. As the sample is cooled from the paramagnetic state into the domain state, the system is expected to remain in equilibrium for $T>T_M(H)$ and random-field critical behavior should be observable within a certain temperature range above $T_M$. From the correlation length measured by neutron scattering above $T_M(H)$, one may extract the

 

exponent $\nu$ of the RFIM, where $\kappa \sim t^{-\nu}$ and $t = T/T_N - 1$ and even extrapolate the equilibrium random-field Néel temperature $T_N(H)$, assuming the existence of a second order phase transition. This approach has been attempted previously by several workers[7,6] and the values of several random-field critical exponents were estimated, though the metastability temperature was not well defined in these studies and in certain cases there were signs of contamination from random exchange crossover behavior either due to weak random-field strength or inappropriate temperature ranges. In the present work, we pursue such an approach through a double-axis neutron scattering study on the prototypical DAFF $Fe_{0.5}Zn_{0.5}F_2$ in a field and measure the correlation length above $T_M(H)$ but below the zero field $T_N$. From the data, we extract the equilibrium correlation length exponent $\nu$, the connected susceptibility exponent $\gamma$, the disconnected susceptibility exponent $\bar{\gamma}$, and the equilibrium random-field transition temperature $T_N(H)$. We compare these values with previous experimental results and current theoretical estimates.

The advent of synchrotron magnetic x-ray scattering has brought new excitement to RFIM research. As discussed in the preceding paper, it has proven to be an ideal tool for measuring the order parameter in the ZFC transition,[12,26,23] and has also led to unexpected discoveries on field cooling. In a magnetic x-ray scattering study on a sample of $Mn_{0.75}Zn_{0.25}F_2$, Hill *et al.* observed long range ordering in the field-cooled state,[29,12] in apparent contradiction with neutron scattering results for which field-cooled long range order was not observed. To date, however, this remains the only evidence of long range magnetic order in a field-cooled DAFF and it is therefore important to investigate further this unexpected phenomenon. As reported in Hill *et al.*, the two $Mn_{0.75}Zn_{0.25}F_2$ samples studied exhibited different ordering behavior. In one sample, labeled the SRO sample, hysteretic behavior similar to that seen by neutron scattering was observed—that is, LRO in the ZFC state and only SRO in the FC state. However, another sample, labeled the LRO sample and obtained from the same boule as the first sample, displayed LRO in the FC state as well as in the ZFC state. Data taken in the FC state of this sample revealed a coexistence of LRO and SRO; the line shape exhibited a resolution limited component with diffuse tails. The intensity of LRO was smaller than that of the ZFC state. At $H = 6$ T, it was estimated that approximately one-half of the illuminated volume achieved long range order on field cooling.

Several important results emerged from the x-ray study of the LRO $Mn_{0.75}Zn_{0.25}F_2$ sample.[29,12] The measurements suggested that the observed LRO came from the near surface region of the sample, which dominates the signal in an x-ray experiment but makes a vanishingly small contribution to the neutron scattering. The temperature dependence of the FC LRO intensity was found to fit to a power law, $I \sim t^{2\beta}$, with $\beta_{FC} \approx 0.3$, which is close to the random exchange Ising value; and the long range order was observed to develop at a temperature, labeled $T_N(H)$, below the metastability boundary, $T_M(H)$. At $H = 6$ T, $T_M - T_N \approx 1.2$ K. The differences in the results from the two x-ray samples were attributed to the difference in their surface qualities that resulted from different polishing processes. The LRO sample went through a less refined polishing and exhibited a surface with significantly more scratches than the SRO sample. Several possibilities were suggested to explain how the surface defects might have nucleated ordering, for example by producing an asymmetric distribution of the random fields in the near surface region.

In the present work, we have carried out an x-ray scattering study of two different DAFF's $Fe_{0.5}Zn_{0.5}F_2$ and $Mn_{0.45}Zn_{0.55}F_2$, in order to address the following questions. First, is the FC LRO unique to the LRO sample of $Mn_{0.75}Zn_{0.25}F_2$, or a feature of weakly anisotropic Ising systems, or is it more universal? Second, what are the temperature and field dependences of the LRO and SRO that coexist in the field-cooled state?

## II. EXPERIMENTAL DETAILS

Both $FeF_2$ and $MnF_2$ have the rutile-type structure and a uniaxial magnetic anisotropy in the $c$ direction. The anisotropy in $FeF_2$ originates from crystal fields and is of comparable strength to the exchange interaction. In $MnF_2$, the anisotropy arises from the dipolar interaction and its strength is approximately 1% of the exchange. As a result of this difference, $Fe_xZn_{1-x}F_2$ and $Mn_xZn_{1-x}F_2$ have been widely studied as models of the 3D RFIM with strong and weak anisotropies, respectively.

The $Fe_{0.5}Zn_{0.5}F_2$ and $Mn_{0.45}Zn_{0.55}F_2$ crystals used in the current studies were grown using the Czochralski method. The room temperature lattice constants for $Fe_{0.5}Zn_{0.5}F_2$ are $a = b = 4.71$ Å and $c = 3.24$ Å, while those for $Mn_{0.45}Zn_{0.55}F_2$ are $a = b = 4.87$ Å and $c = 3.31$ Å. Both the $Fe_{0.5}Zn_{0.5}F_2$ samples used in the neutron and x-ray experiments were cut from the same-boule. Careful attention was paid to the polishing of the x-ray samples. Both the $Fe_{0.5}Zn_{0.5}F_2$ and the $Mn_{0.45}Zn_{0.55}F_2$ crystals went through a preparation process similar to that applied to the SRO sample of $Mn_{0.75}Zn_{0.25}F_2$ which had a smooth surface with well-separated scratches. The crystal surfaces were polished on a polishing wheel covered with *Buehler* felt and lubricant, using successively finer grits in each step of the procedure. The final polishing was accomplished with 0.05 $\mu$m alumina powder on *Polytek Supreme* felt. Scanning electron microscopy showed that the polishing left some scratches on the sample surfaces, typically of approximately 0.1 $\mu$m in width. The surface quality is in general very similar to that of the SRO $Mn_{0.75}Zn_{0.25}F_2$ sample.[12]

The concentration homogeneity of the two samples is reflected in the sharpness of the zero-field transition. The transition broadening is approximately 0.15 and 0.1 K half width at half maxima (HWHM) [modeling the x-ray measured order parameters by a Gaussian-broadened power law, Eq. (3)], corresponding to a concentration variation of $\Delta x < 3 \times 10^{-3}$ over the illuminated volume, for the $Mn_{0.45}Zn_{0.55}F_2$ and the $Fe_{0.5}Zn_{0.5}F_2$ samples, respectively. The penetration depth of the x rays is approximately 3.5 $\mu$m. The crystallographic quality of the samples is illustrated by the transverse scan profile of the x-ray charge scattering peaks. At (200), the measured mosaic spread is 0.006° HWHM for both samples.

The neutron scattering experiments were carried out on spectrometer H7 at the Brookhaven High Flux Beam Reactor. The data were taken in the energy integrating two-axis mode with incident energy of 14.7 meV and collimators of

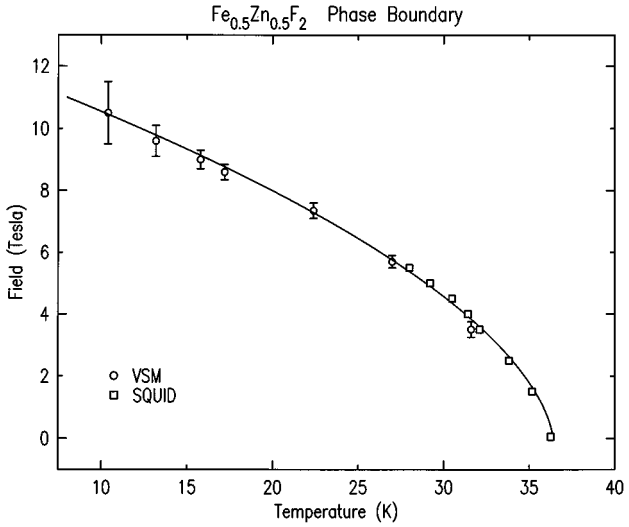


FIG. 1. Phase boundary of $Fe_{0.5}Zn_{0.5}F_2$ as measured by SQUID, open squares, and vibrating sample magnetometry, open circles. Generally, a ZFC procedure was used. The solid line is a guide to the eye.

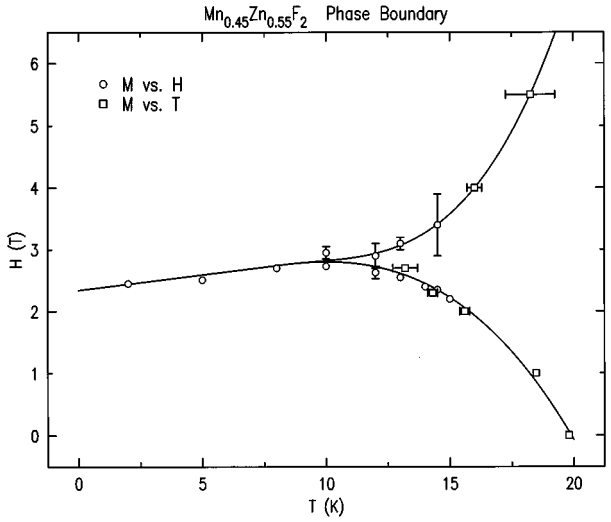


FIG. 2. Phase boundary of $Mn_{0.45}Zn_{0.55}F_2$ as measured by SQUID magnetometry. The open circles and the open squares depict peak positions of field and thermal derivatives of the uniform magnetization, respectively. The solid lines are guides to the eye.

10′-10′-sample-10′. The resulting HWHM resolutions at the (100) Bragg reflection, were 0.0036 reciprocal lattice units longitudinal, 0.0010 reciprocal lattice units transverse in-plane, and 0.025 reciprocal lattice units vertical. Pyrolitic graphite filters were used to remove the higher harmonic contamination from the beam. The sample was mounted inside a superconducting magnet capable of fields up to 6.1 T.

The x-ray experiments were performed on Beamline X20A at the National Synchrotron Light Source. This beamline utilized a platinum coated, bent silicon mirror to focus the x-ray beam horizontally and vertically to a spot of approximate dimensions 1 mm by 1 mm, at the sample position. The mirror also removed the higher harmonic contamination from the beam. For each experiment, the x-ray energy was chosen to minimize the multiple scattering intensity at the magnetic peak position (100). The double-bounce monochromator and the analyzer utilized single crystals of Ge(111). The in-plane resolutions were approximately $4\times10^{-4}$ reciprocal lattice units (HWHM) and $5\times10^{-5}$ reciprocal lattice units in the longitudinal and transverse direction respectively. The vertical resolution, controlled by collimating slits, was $\sim1\times10^{-3}$ reciprocal lattice units. The x-ray scattering spectrometer had an inherent energy resolution of $\sim$10 eV. The samples were mounted in an x-ray compatible superconducting magnet. The alignment between the *c* axis of the samples and the vertical field was better than 3° in both the x-ray and neutron experiments.

Figures 1 and 2 illustrate the phase diagrams of $Fe_{0.5}Zn_{0.5}F_2$ and $Mn_{0.45}Zn_{0.55}F_2$, respectively.[30] The phase boundary of $Fe_{0.5}Zn_{0.5}F_2$ was measured by SQUID magnetometry and high field vibrating sample magnetometry. The transition was identified from peaks in the temperature derivatives and the field derivatives of the measured uniform magnetization. The data were taken starting from a zero field state and then following a ZFC procedure, in the case of the temperature sweeps, or raising the field at fixed temperature in the case of the field sweeps. The phase boundary of $Mn_{0.45}Zn_{0.55}F_2$ was similarly determined by SQUID magnetometry through peaks in the temperature or field derivatives of the uniform magnetization. In general our results agree with those determined from neutron scattering measurements by Cowley *et al.*[6] who found that this phase boundary, though consistent with the expected bicritical geometry, has the property that the scan profiles obtained when the sample is taken from the spin-flop phase into the Ising phase by lowering the external field exhibit a short range order component. This was also seen in our x-ray data. This behavior differs from that of $Mn_{0.75}Zn_{0.25}F_2$, for which a first-order transition clearly divides the spin-flop phase and the Ising phase. Long range order is then achieved when the field is lowered into the Ising phase.

## III. NEUTRON SCATTERING RESULTS

We first report neutron scattering results taken on $Fe_{0.5}Zn_{0.5}F_2$ at $H=5$ and 6 T. In Figs. 3 and 4, representative transverse neutron scattering scans taken at 5 and 6 T, respectively, are shown. All the data were taken above the metastability temperature, $T_M(H)$, at the respective fields. As the temperature is decreased, the scattered intensity increases and the scan profiles become sharper, though they remain much broader than the resolution limit. Typically, the neutron scattering cross section for RFIM systems is taken to be[31]

$$\mathcal{S}(\mathbf{Q})=C\,\delta(\mathbf{q})+\frac{B}{\kappa^2+q^2}+\frac{A\kappa}{(\kappa^2+q^2)^2}+\frac{B_T}{\kappa_T{}^2+q^2}, \quad (1)$$

where $\mathbf{q}=\mathbf{Q}-(100)$. The $\delta$ function represents the long range magnetic order component. The second term corresponds to the longitudinal dynamic susceptibility. The Lorentzian-squared term arises from static fluctuations due to the quenched random-field susceptibility. Written in this form, *A* is the integrated intensity for these fluctuations. The last term corresponds to the transverse dynamic susceptibility. From the fluctuation dissipation theorem, the structure factor $S(\mathbf{Q})$ of Eq. (1) may be written as the sum of two terms,

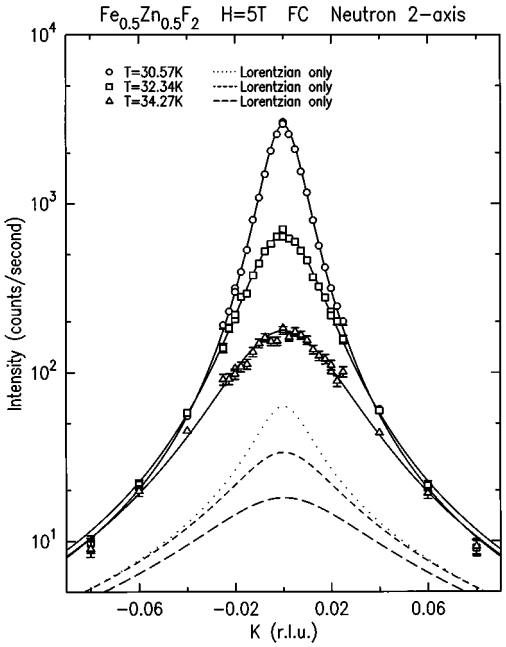


FIG. 3. Transverse neutron scans taken with $Fe_{0.5}Zn_{0.5}F_2$ at three temperatures 30.57, 32.34, and 34.27 K above $T_M$ at 5 T. The solid lines are the results of fits to Eq. (1) convoluted with the instrumental resolution function. The dotted, short-dashed, and long-dashed lines are the dynamic Lorentzian susceptibility components of the structure factor for the three respective temperatures.

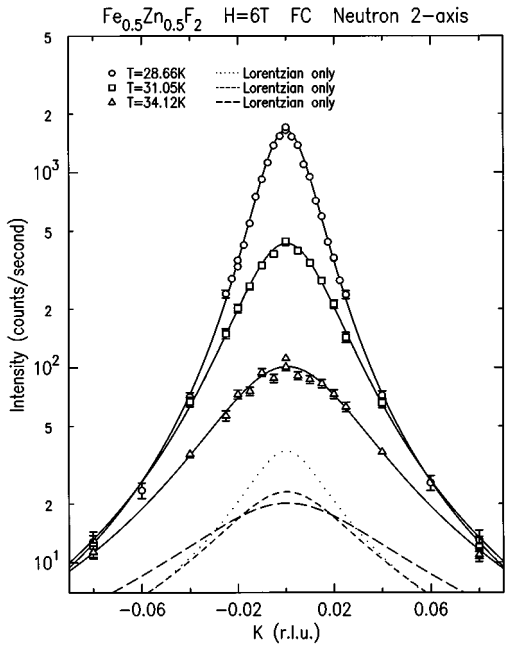


FIG. 4. Transverse neutron scans taken with $Fe_{0.5}Zn_{0.5}F_2$ at three temperatures 28.66, 31.05, and 34.12 K above $T_M$ at 6 T. The solid lines are the results of fits to Eq. (1) convoluted with the instrumental resolution function. The dotted, short-dashed, and long-dashed lines are the dynamic Lorentzian susceptibility components of the structure factor for the three respective temperatures.

$S(\mathbf{Q})=T\chi(\mathbf{Q})+T\chi_{\rm dis}(\mathbf{Q})$, where $\chi_{\rm dis}=\Sigma_j\langle\sigma_0\rangle\langle\sigma_j\rangle$ and $\chi=\Sigma_j[\langle\sigma_0\sigma_j\rangle-\langle\sigma_0\rangle\langle\sigma_j\rangle]$ are the so-called disconnected and connected susceptibilities, respectively. In a nonrandom system, for $T>T_C$, $\Sigma_j\langle\sigma_0\rangle\langle\sigma_j\rangle=0$, and $S(0)\sim T\chi\sim t^{-\gamma}$. However, in random systems $\chi_{\rm dis}$ is no longer zero and a new exponent is defined, $\chi_{\rm dis}\sim t^{-\overline{\gamma}}$. In the following, we will obtain experimental values for $\gamma$ and $\overline{\gamma}$, together with the correlation length exponent $\nu$, where $1/\kappa\sim t^{-\nu}$. In Eq. (1), we identify the thermal fluctuations, given by the parameters $B$ and $B_T$, with $\chi(\mathbf{Q})$ and the random-field fluctuations, $A$, with $\chi_{\rm dis}(\mathbf{Q})$. The DAFF systems studied here possess a $c$-axis uniaxial anisotropy and the transverse susceptibility is typically much smaller than the longitudinal susceptibility. This is particularly true for $Fe_{0.5}Zn_{0.5}F_2$ which has a large anisotropy. Further, $B_T$ and $\kappa_T$ vary only slowly with temperature and do not exhibit critical behavior.[32] The transverse term has therefore been neglected in $\mathcal{S}(\mathbf{Q})$ in the analysis. For data taken on field cooling, there is no resolution-limited LRO component, and these data were therefore analyzed by fitting to the sum of the longitudinal Lorentzian and the static Lorentzian squared terms in $\mathcal{S}(\mathbf{Q})$ convolved with the instrumental resolution. The fits from such an analysis result in the solid lines shown in Figs. 3 and 4.

From the parameters $\kappa$, $A$, and $B$, one may extract the correlation length $\xi\sim 1/\kappa$, the connected susceptibility $\chi\sim B/\kappa^2$, and the disconnected susceptibility $\chi_{\rm dis}\sim A/\kappa^3$. Assuming that these parameters reflect the approach toward an equilibrium second order transition, one can obtain the equilibrium exponents $\nu$, $\gamma$, and $\overline{\gamma}$ provided that one uses data taken above $T_M(H)$. In the current study, $T_M(H)$ is defined unambiguously; it is the temperature at which the ZFC long range order goes to zero. Above this temperature, the system is in equilibrium and exhibits no hysteresis. Note that $T_M(H)$ is different from the *trompe l'oeil* pseudocritical temperature of the ZFC transition, $T_C(H)$, where the ZFC critical scattering intensity peaks and the ZFC correlation length reaches a finite maximum. Below $T_M(H)$, random-field dynamics dominate the behavior, as the system becomes trapped in local free energy minima and unable to relax fully. Between $T_M(H)$ and a crossover temperature of order $T_N(0)=37.6$ K, one expects new critical behavior, that of the RFIM. Here the system is in equilibrium and one may measure the critical properties in the usual fashion.

It was found that $\kappa$, $\chi_{\rm dis}$, and $\chi$ could indeed be described by simple power laws, for both $H=5.0$ and 6.0 T. From $\kappa$, least squares fits yield $\nu(5\ \mathrm{T})=1.59\pm0.14$ and $\nu(6\ \mathrm{T})=1.44\pm0.27$ and we conclude that $\nu=1.5\pm0.3$. In fact, holding $\nu$ constant at this value results in satisfactory fits to the data, as illustrated by the solid lines in the top panels of Figs. 5 and 6, which represent fits with $\nu=1.5$. Note that this value of $\nu$ is significantly larger than 1, in agreement with current theoretical estimates.[33,1,34] The transition temperature, $T_N(H)$, of the power law fits was treated as an adjustable parameter and represents the underlying equilibrium random-field critical point, which the system is not able to reach, at least in the bulk, due to the slow dynamics. The arrows in Figs. 5 and 6 indicate the positions of $T_N(H)$, which lie substantially below $T_M(H)$. At $H=5.0$ T $T_M(5\ \mathrm{T})-T_N(5\ \mathrm{T})\approx3.4$ K, and for $H=6.0$ T, $T_M(6\ \mathrm{T})-T_N(6\ \mathrm{T})\approx5.8$ K. A preliminary analysis for data at lower fields shows that $T_M(H)-T_N(H)$ increases smoothly with increasing field.

As the temperature is decreased toward $T_M(H)$, $\chi_{\rm dis}$ and $\chi$ grow dramatically. We found that meaningful least squares fits could be obtained only by fixing $T_N(H)$ at the values

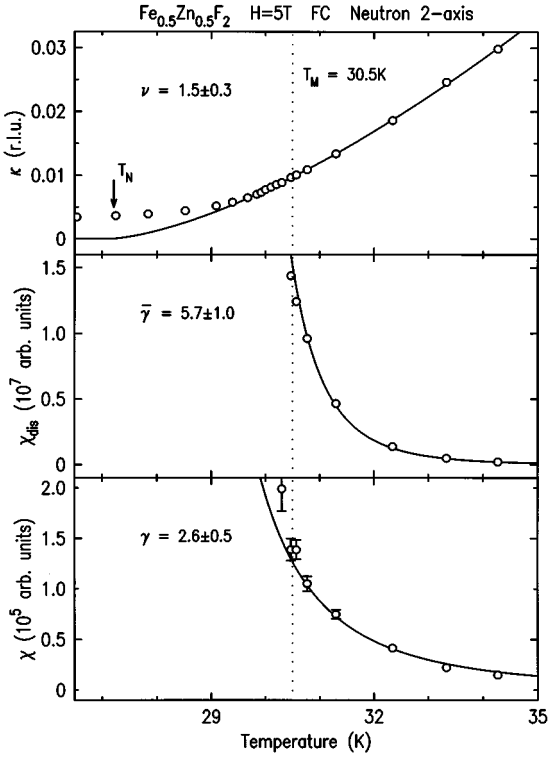


FIG. 5. Inverse correlation length $\kappa$, disconnected susceptibility $\chi_{\rm dis}$, and connected susceptibility $\chi$ as measured by neutron scattering for $Fe_{0.5}Zn_{0.5}F_2$ at 5 T. The dotted line shows the metastability temperature. $T_N$ is the temperature at which the solid line fit for $\kappa$ reaches zero. The estimated critical exponents are given.

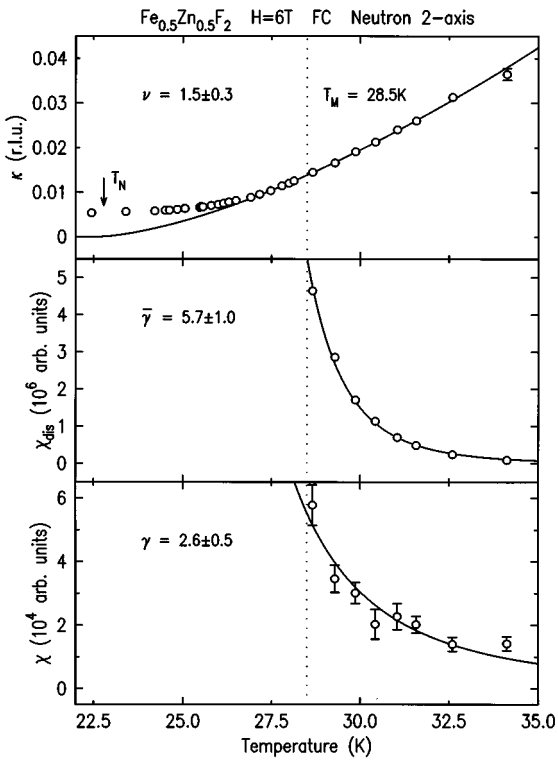


FIG. 6. Inverse correlation length $\kappa$, disconnected susceptibility $\chi_{\rm dis}$, and connected susceptibility $\chi$ as measured by neutron scattering for $Fe_{0.5}Zn_{0.5}F_2$ at 6 T. The dotted line shows the metastability temperature. $T_N$ is the temperature at which the solid line fit for $\kappa$ reaches zero.

determined by the power-law fits of the inverse correlation length, $\kappa$. Following this approach, we estimate $\bar{\gamma}=5.7\pm1$ and $\gamma=2.6\pm0.5$, where the large errors reflect the strong dependence of the exponents on the choice of $T_N$. In the middle and bottom panels of Figs. 5 and 6, $\chi_{\rm dis}$ and $\chi$ are plotted for $H=5$ and 6 T, respectively. The solid lines are power law fits with $T_N$ fixed at the value determined from the fits to $\kappa$, and the exponents $\bar{\gamma}$ and $\gamma$ fixed at 5.7 and 2.6, respectively. We note that these values for $\bar{\gamma}$ and $\gamma$ are considerably larger than those previously reported, but are consistent within the combined experimental and theoretical errors with most current theoretical predictions.[35,34]

## IV. MAGNETIC X-RAY SCATTERING RESULTS

As a result of the small scattering cross section and high resolution, magnetic x-ray scattering is well suited to the study of large length scale phenomena, including especially the LRO order parameter. However, the inherent high resolution is a hindrance in the study of diffuse scattering. Therefore, the x-ray measurements reported here were performed at fields below 3 T, for which the magnetic domains are relatively large to facilitate a detailed study of both the long range and short range order. In both $Fe_{0.5}Zn_{0.5}F_2$ and $Mn_{0.45}Zn_{0.55}F_2$, we find a coexistence of LRO and SRO under field cooling for relatively low fields ($\leqslant$2.5 T). The correlation length of the SRO decreases with increasing field, as previously observed by neutron and x-ray scattering.[6,12] Interestingly, the LRO decreases in intensity as the field is increased and becomes unobservable above a threshold field.

The cross section for magnetic x-ray scattering is essentially the same as Eq. (1), with the dynamic susceptibility (Lorentzian) terms set to zero,

$$S(\mathbf{Q})=\frac{A\kappa}{(\kappa^2+\mathbf{q}^2)^2}+C\delta(\mathbf{q}). \tag{2}$$

Again, $C$ is the intensity of long range magnetic order and is proportional to the staggered magnetization squared, $M_S^2$. $A$ is the integrated intensity of the short range order. The dynamic susceptibility terms are neglected because the random-field term (Lorentzian squared) dominates the x-ray diffuse scattering. As was the case for the earlier study of $Mn_{0.75}Zn_{0.25}F_2$ the scan profiles were adequately described by Eq. (2), convolved with the resolution function. In the present x-ray data analysis, the convolution integral was carried out only in the transverse ($K$) direction. This is because the diffuse scattering in the longitudinal ($H$) scans was found, unexpectedly, to be asymmetric with respect to the central $\delta$-function peak. The results are therefore qualitatively, but not necessarily quantitatively correct.

### A. $Fe_{0.5}Zn_{0.5}F_2$

A detailed study of the temperature dependence of the LRO and SRO has been carried out at $H=1.5$ and 1 T on $Fe_{0.5}Zn_{0.5}F_2$. Figure 7 shows transverse and longitudinal scans at $T=15$ K and $H=1.5$ T. The ZFC scans are resolution limited in both directions and this is the case for all temperatures below $T_M$. The peak in the background results

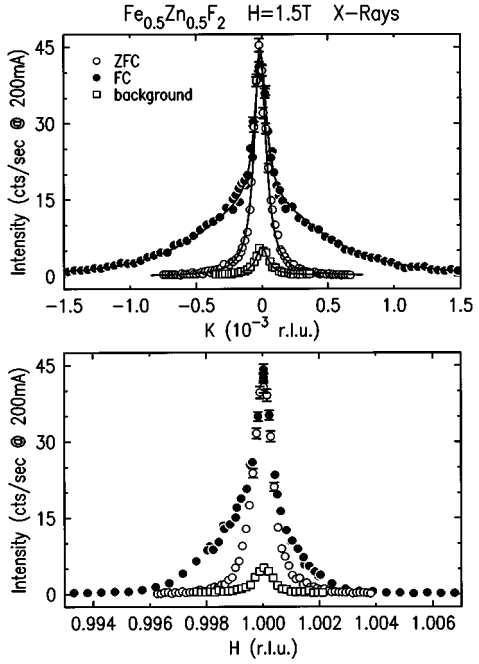


FIG. 7. Representative ZFC (open circles), FC (closed circles), and multiple scattering background (open squares) scans at $H=1.5$ T and $T=15$ K for $Fe_{0.5}Zn_{0.5}F_2$ as measured by magnetic x-ray scattering. Upper panel: transverse scans. The solid lines are the results of least squares fits to Eq. (2). Lower panel: longitudinal scans. Note that the FC scan is asymmetric due to an offset in the peaks of the two components. The ZFC scans and the multiple scattering scans are all resolution limited. The ZFC data have been scaled to match the FC peak intensity for comparison.

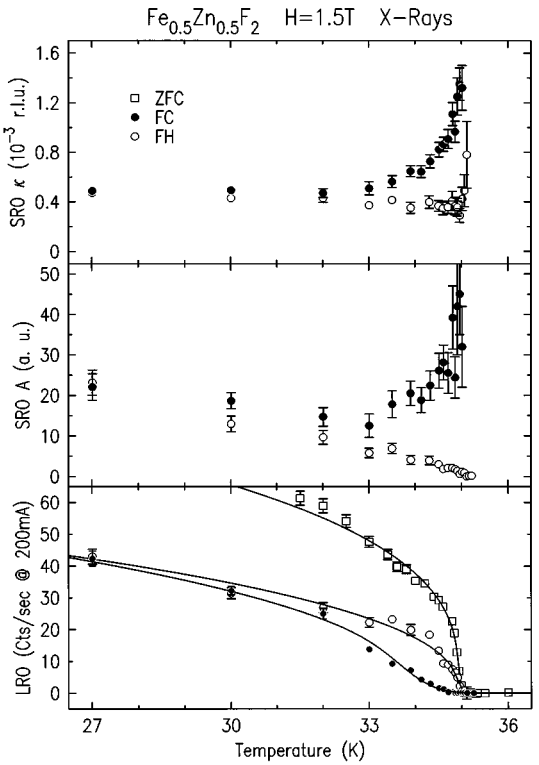


FIG. 8. Comparison of ZFC (open squares), FC (closed circles), and FH (open circles) parameters of $Fe_{0.5}Zn_{0.5}F_2$ at $H=1.5$ T as measured by x rays. Top panel: inverse correlation length ($\kappa$) of SRO. Middle panel: integrated intensity ($A$) of SRO. Bottom panel: LRO component. The solid lines are the results of least squares fits to Eq. (3).

from multiple scattering processes. The latter are temperature independent and are subtracted off in the data analysis. The FC transverse scan displays a resolution-limited central peak together with a broad diffuse peak resulting from short range magnetic order. Note that the ZFC data have been scaled by a factor of 0.25 to have the same peak intensity as the FC data, to facilitate comparison. The profile is well described by Eq. (2) (solid line). The FC longitudinal scan similarly suggests two length scales, though the two peaks appear to be slightly offset from each other. This unexpected feature was also seen in $Mn_{0.45}Zn_{0.55}F_2$, but was not observed in previous studies on $Mn_{0.75}Zn_{0.25}F_2$. A temperature cycle of ZFC, followed by FC and then field heating (FH) was performed at $H=1.5$ T and the fitted parameters for the LRO intensity, SRO inverse correlation length $\kappa$, and SRO integrated intensity $A$ are summarized in Fig. 8. The bottom panel compares the ZFC, FC, and FH long range order intensity. The temperature dependence of the ZFC long range order is fitted to a Gaussian-rounded power law,[12]

$$I(T,H)=\frac{1}{\sqrt{\pi\sigma_{\mathrm{ZFC}}^2(H)}}\int\left(\frac{t_c-T}{t_c}\right)^{2\beta}\times\exp\left[-\left(\frac{t_c-T_c(H)}{\sigma_{\mathrm{ZFC}}(H)}\right)^2\right]dt_c\,. \qquad (3)$$

The parameter $\sigma$ provides a measure of the random-field induced rounding at the ZFC transition. This is labeled ''trompe l'oeil'' critical behavior in Ref. 12 since $I(T,H)$ simulates a rounded second order transition even though the diminution of the intensity occurs primarily in the superheated temperature region above $T_N(H)$. The fit yields $\beta_{\mathrm{ZFC}}(1.5\ \mathrm{T})=0.19\pm0.03$, $\sigma_{\mathrm{ZFC}}(1.5\ \mathrm{T})=0.09\pm0.03$ K, and $T_C(1.5\ \mathrm{T})=34.95\pm0.1$ K. Upon field cooling, a LRO component starts to appear at approximately 0.3 K below $T_M(1.5$ T). This agrees with our observations on $Mn_{0.75}Zn_{0.25}F_2$.[12] The rise of the FC LRO appears very rounded. Fitting it to Eq. (3) yields $\beta_{\mathrm{FC}}(1.5\ \mathrm{T})=0.27\pm0.06$, with a large $\sigma_{\mathrm{FC}}(1.5$ T)$=0.65\pm0.1$ K. The center of the Gaussian distribution is at $T_{C,\mathrm{FC}}(1.5\ \mathrm{T})=34.2\pm0.2$ K, approximately 0.8 K below the ZFC $T_C$ at 1.5 T. The FH LRO intensity, measured subsequent to a FC protocol, rises above the FC LRO and its temperature dependence is remarkably similar to the ZFC LRO at 1.5 T. It reaches zero at exactly $T_M$ and is described by $\beta_{\mathrm{FH}}(1.5\ \mathrm{T})=0.21\pm0.03$, $\sigma_{\mathrm{FH}}(1.5\ \mathrm{T})=0.13\pm0.03$ K, and $T_{C,\mathrm{FC}}(1.5\ \mathrm{T})=34.95\pm0.1$ K when fitted to Eq. (3). The FH transition for the long range ordered component thus appears to be proceed via the same mechanism as the superheated ZFC transition.

In the top panel of Fig. 8, the FC and FH inverse correlation lengths, $\kappa$, are plotted. The FC $\kappa$ decreases sharply as the sample is cooled through the metastability transition and gradually saturates at low temperatures. Upon subsequent heating, the FH correlation length stays constant up to $T_C(1.5$ T), defined in Eq. (3) for the ZFC transition. This is in agreement with previous neutron scattering observations.[5,11] The integrated intensity of the SRO compo-

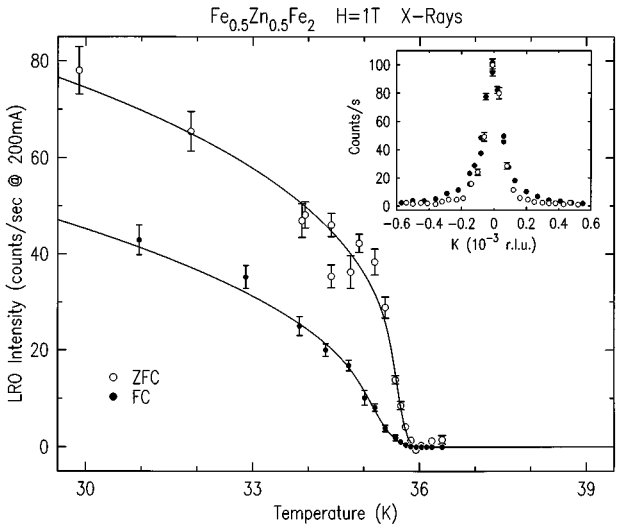


FIG. 9. Comparison of ZFC and FC LRO at 1 T in $Fe_{0.5}Zn_{0.5}F_2$ as measured by magnetic x-ray scattering. The solid lines are the results of least squares fits to Eq. (3), yielding $\beta_{ZFC}=0.17\pm0.03$ and $\beta_{FC}=0.25\pm0.04$.

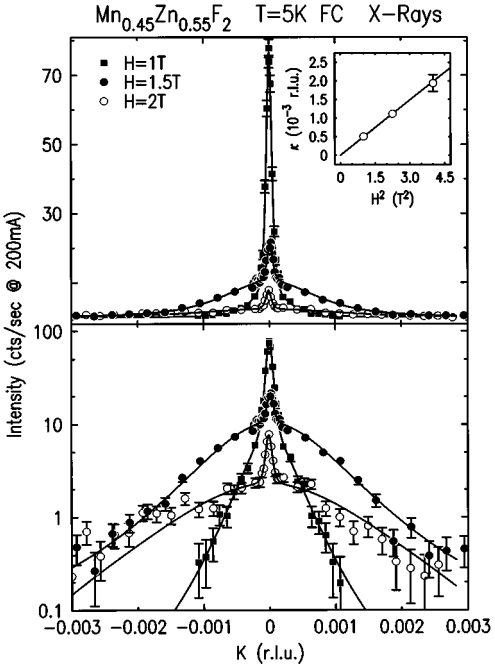


FIG. 10. FC x-ray scans well below $T_C(H)$ at $H=1$ T (closed squares), 1.5 T (closed circles), and 2 T (open circles) for $Mn_{0.45}Zn_{0.55}F_2$. The scans show a sharp decrease in the LRO intensity and a broadening of the SRO tails with increasing fields. The bottom panel shows the same data on a semilogarithmic plot. The inset plots the FC $\kappa$ vs $H^2$.

nent is plotted in the middle panel. The intensity behaves quite differently during FC and FH cycles. Summarizing, the FH state has a larger long range ordered component and a larger domain size relative to that of the FC state.

A similar analysis was carried out for the x-ray data taken at $H=1$ T. In Fig. 9, we compare the ZFC and FC LRO measured at $H=1$ T. As the temperature decreases under a FC protocol, the LRO component is seen to appear in a rather rounded fashion, at a temperature indistinguishable from that at which the ZFC LRO reaches zero. Fitting the FC LRO to Eq. (3) yields $\beta_{FC}(1\text{ T})=0.26\pm0.05$, $\sigma_{FC}(1\text{ T})=0.37\pm0.06$ K, and the Gaussian distribution centers at $35.3\pm0.1$ K; this is to be compared with $\beta_{ZFC}(1\text{ T})=0.17\pm0.03$ and the ZFC $T_C(1\text{ T})=35.6\pm0.1$ K obtained from fitting the ZFC order parameter to a simple power law or to the rounded power law with a small $\sigma$. The FC LRO component is significantly stronger than that at $H=1.5$ T and dominates the scattered intensity in the FC state, as shown by a comparison of the ZFC and FC transverse scans at 15 K in the inset, in which the peak intensities of the two scans have been normalized to agree with one another.

### B. $Mn_{0.45}Zn_{0.55}F_2$

Figure 10 shows FC transverse scans taken at $H=1$, 1.5, and 2 T at temperatures well below $T_C(H)$ on the $Mn_{0.45}Zn_{0.55}F_2$ sample. Again, a LRO FC component is observed in the x-ray data. The peak intensity of the scans decreases drastically at higher fields. The LRO component decreases from 62 counts/s at $H=1$ T to 7 counts/s at $H=1.5$ T, and all but disappears at $H=2$ T. Above 2.5 T, the FC state exhibits no observable long range ordered component, only SRO diffuse scattering. At the same time, the Lorentzian squared diffuse tails broaden, as is more clearly illustrated in the semilogarithmic plot in the bottom panel of Fig. 10. The FC inverse correlation length, $\kappa$, appears to be proportional to $H^2$, as shown in the inset. This is in agreement with neutron scattering results on $Fe_{1-x}Zn_xF_2$ that showed the FC $\kappa$ to scale with $H^{2.2\pm0.1}$,[5] but disagrees with those on $Mn_{0.5}Zn_{0.5}F_2$ ($\nu_H=3.4\pm0.4$) and $Mn_{0.75}Zn_{0.25}F_2$ ($\nu_H=3.3\pm0.8$).[6] All of the neutron results were taken at larger fields and correspondingly larger $\kappa$'s.

The temperature dependence of the LRO and SRO was measured during ZFC, FC, and FH runs at $H=1$ and 1.5 T. Figure 11 compares the LRO amplitude in the ZFC and the FC states for $H=1$ T. The ZFC intensity is again well described by Eq. (3) with $\beta_{ZFC}(1\text{ T})=0.18\pm0.03$ and $\sigma_{ZFC}(1\text{ T})=0.13\pm0.02$ K. The zero-field-cooled $T_C(1\text{ T})=18.2\pm0.1$

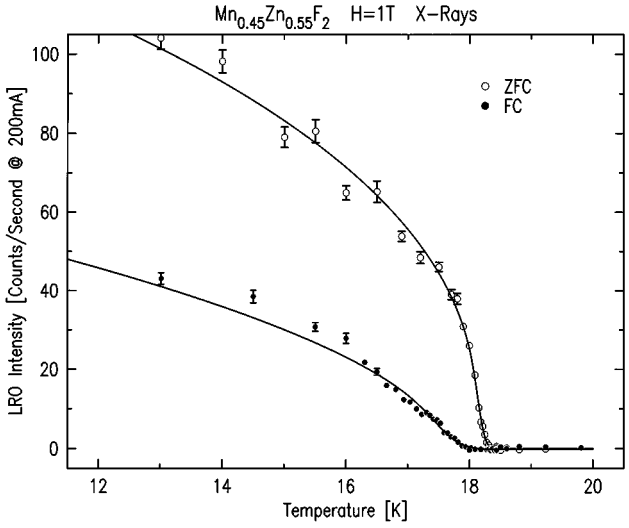


FIG. 11. ZFC and FC LRO of $Mn_{0.45}Zn_{0.55}F_2$ at $H=1$ T as measured by magnetic x-ray scattering.

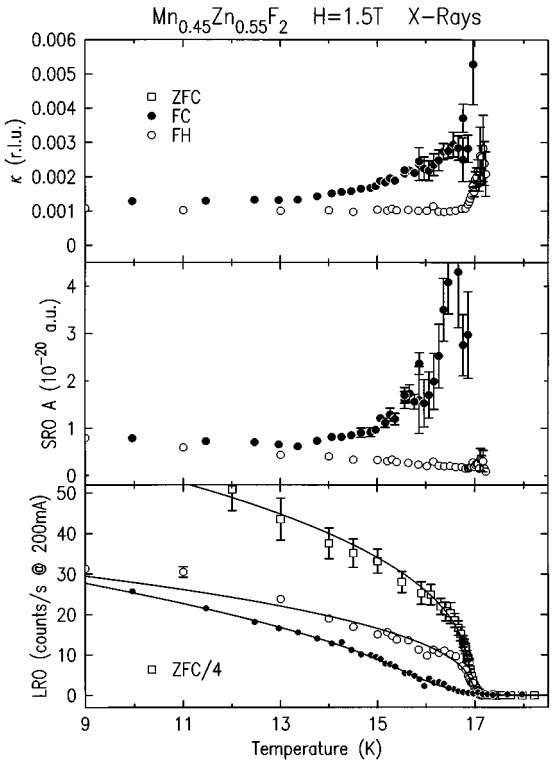


FIG. 12. Comparison of ZFC (open squares), FC (closed circles), and FH (open circles) parameters of $Mn_{0.45}Zn_{0.55}F_2$ at $H=1.5$ T as measured by x rays. Top panel: inverse correlation length ($\kappa$) of the SRO. Middle panel: integrated intensity ($A$) of the SRO. Bottom panel: LRO component. The solid lines are the results of least squares fits to power laws, as described in the text.

K. The same fitting function yields $\beta_{FC}(1\text{ T})=0.28\pm0.04$ and a distribution width of $\sigma_{FC}(1\text{ T})=0.4\pm0.1$ K around $T_{C,FC}(1\text{ T})=17.7\pm0.1$ K for the FC LRO intensity. Note also that the FC LRO develops at approximately 0.4 K below $T_M(1\text{ T})\approx18.3$ K.

As shown in Fig. 10, the FC intensity at $H=1$ T is dominated by the LRO. At $H=1.5$ T, $\kappa$ is larger, the LRO and SRO peak amplitudes are comparable and fitting the scans to two peaks of different length scales therefore yields more reliable parameters. Figure 12 summarizes the ZFC, FC, and FH parameters at $H=1.5$ T.

The general features of $\kappa$, $A$, and the LRO are essentially similar to those found in $Fe_{0.5}Zn_{0.5}F_2$. The hysteretic effects agree qualitatively with those observed by neutron scattering[5,6] and earlier magnetic x-ray scattering experiments on DAFF's including $Mn_xZn_{1-x}F_2$.[29,12] The FH $\kappa$ remains smaller than the FC $\kappa$ up to $T_M(1.5\text{ T})$, though there is a marked broadening at $T_C(1.5\text{ T})$. Beyond $T_M(H)$ the intensity becomes too low for accurate measurements by x rays. The SRO integrated intensity also decreases significantly during field heating, while it remains roughly constant during field cooling. The ZFC transition is characterized by $\beta_{ZFC}(1.5\text{ T})=0.19\pm0.03$, $\sigma=0.14\pm0.03$ K, and $T_M(1.5\text{ T})\approx17.2$ K. The FC LRO appears at $T=16.8$ K, 0.4 K below $T_M(1.5\text{ T})$, and again rises in a severely rounded fashion. Fitting it to Eq. (3) yields $\beta_{FC}(1.5\text{ T})=0.31\pm0.04$, $\sigma_{FC}(1.5\text{ T})=1\pm0.2$ K, and $T_{C,FC}(1.5\text{ T})=16.3\pm0.2$ K, approximately 0.8 K below $T_{C,ZFC}$. The FH LRO intensity, on the other hand, resembles that of the ZFC intensity except for its smaller amplitude. Fitting these data with Eq. (3) yields $\beta_{FH}=0.20\pm0.03$ and $\sigma=0.12\pm0.03$ K, both comparable to the ZFC fitted parameters. Further, the FH LRO component remains observable up to within 0.1 K of $T_M(1.5\text{ T})$, where the ZFC LRO diminishes to zero.

## V. DISCUSSION

The combined neutron and x-ray scattering data presented above suggest the existence of an equilibrium random-field transition at $T_N(H)$, which lies below the metastability temperature $T_M(H)$ and the *trompe l'oeil* ZFC transition temperature $T_C(H)$. This is implicit in the neutron scattering data, where the correlation length, connected and disconnected susceptibilities all demonstrate power law behavior in the equilibrium regime above $T_M(H)$, with a singularity at $T_N(H)$. However, as a consequence of the random-field activated dynamics, the measured FC $\kappa$ deviates from the power law behavior well before the temperature reaches $T_N(H)$. In the second half of the paper, we reported the observation of a field-cooled transition to long range order as observed by x-ray scattering at a temperature below $T_M(H)$. These latter data were taken at lower fields. It seems natural also to identify this temperature with $T_N(H)$, though we cannot make a direct comparison between the neutron and x-ray results due to the differences in applied fields.

Besides predicting $T_N(H)$, the neutron data also yield estimates for the critical exponents of the RFIM; $\nu=1.5\pm0.3$, $\gamma=2.6\pm0.5$, and $\overline{\gamma}=5.7\pm1$. Similar approaches have been taken previously with neutron measurements. For example, Belanger *et al.* estimated $\nu=1.0\pm0.15$, $\gamma=1.75\pm0.2$, and $\overline{\gamma}=3.5$, from data taken at $H=1.4$ and 2 T on $Fe_{0.6}Zn_{0.4}F_2$.[7] These authors thus suggested that the 3D RFIM exhibited 2D pure Ising critical behavior. We believe the apparent discrepancy between these estimates and our current results is mainly due to the crossover to random exchange criticality at small random fields in the earlier $Fe_{0.6}Zn_{0.4}F_2$ study. The effective random field strength at 2 T in $Fe_{0.6}Zn_{0.4}F_2$ is much smaller than that in a $x=0.5$ sample at the same applied field, due to the smaller dilution of Zn.[23] With such weak random fields, one expects random exchange crossover behavior and this may explain the smaller value of $\nu$ reported. In fact, Yoshizawa *et al.*[11] examined the same data on $Fe_{0.6}Zn_{0.4}F_2$ and concluded they were not sufficient for making statements about equilibrium critical exponents.

In an extensive neutron scattering study on $Mn_{0.75}Zn_{0.25}F_2$, Cowley *et al.* carried out a similar approach in order to determine the exponent $\nu$ and the equilibrium Néel temperature.[6] As these authors emphasized, the values of $\nu$ and $T_N(H)$ varied significantly depending on the temperature ranges chosen for the fits. Specifically, fits limited to data below $T_N(0)$ yielded values of $\nu$ that were substantially above 1, while including data at higher temperatures in the fits brought the value closer to 1. This again presumably reflects random exchange crossover effects. The authors thus concluded that $\nu=1.4\pm0.3$ and excluded the possibility of $\nu=1$. In the $Mn_{0.75}Zn_{0.25}F_2$ study, data between $T_M(H)$ and $T_{C,ZFC}(H)$ were used in the fits, but this should not have compromised the results significantly. The good agreement between our results for $\nu$ and those of Cowley *et al.* is encouraging.

We believe the current neutron study, performed on the random-field Ising magnet $Fe_{0.5}Zn_{0.5}F_2$ with a crystal of good crystallographic quality, at fields that are amongst the highest used in random-field experiments and restricting the data analysis to the temperature range $[T_M(H), T_N(0)]$, is the most logical approach to studying equilibrium random-field critical behavior. The exponents directly determined from such fits are comparable to current theoretical predictions. For the susceptibilities, recent accurate series expansion calculations by Gofman *et al.*[35] demonstrated two exponent scaling for the RFIM and predicted $\gamma=2.1\pm0.2$ and $\overline{\gamma}=2\gamma$ in 3D. Monte Carlo simulations by Rieger *et al.* yielded $\gamma=2.3\pm0.3$ and $\overline{\gamma}=4.8\pm0.9$ for binary random-field distributions, and $\gamma=1.7\pm0.2$ and $\overline{\gamma}=3.3\pm0.6$ for Gaussian distributions.[36,34] Our measured values of $\gamma$ and $\overline{\gamma}$, though slightly larger, generally agree with these predictions to within the combined errors. They are also consistent with two-exponent random-field scaling which requires that $\overline{\gamma}=2\gamma$. For the correlation length exponent $\nu$, we have the predictions of $\nu=1.6$ by Bruce and Wallace,[37] $\nu=1.3\pm0.3$ by Ogielski and Huse,[38] $\nu=1.4$–$1.5$ by Schwartz,[33] and $\nu=1.6\pm0.3$ and $\nu=1.1\pm0.2$ by Rieger for binary and Gaussian random-field distributions, respectively.[36,34] Our measured $\nu=1.5\pm0.3$ is clearly in agreement with all of these theoretical values within the combined errors. Unfortunately, our results do not differentiate between the various theoretical predictions.

The x-ray data presented here display the following features. First, coexisting long range magnetic order and short range order are observed during field-cooling and subsequent field heating for fields below a certain threshold in both $Mn_{0.45}Zn_{0.55}F_2$ and $Fe_{0.5}Zn_{0.5}F_2$. Second, the intensity of the FC and FH LRO relative to the ZFC LRO amplitude decreases with increasing fields. The destruction of the LRO state following both FH and ZFC protocols for a given field can be described by a rounded power law with the same $\beta$, $T_C$, and $\sigma$. On the other hand, the growth of the FC LRO is generally described by a higher $\beta_{FC}$ that ranges from 0.25 to 0.35, and a much larger rounding. Averaging the fitted $\beta_{FC}$ at all the available fields in both samples, we estimate $\beta_{FC}=0.3\pm0.05$. Further, as noted above, the FC LRO appears at a temperature significantly below $T_M(H)$. During field heating, the system generally retains more order than the FC state at corresponding temperatures, reflected in a higher LRO intensity and a longer correlation length. Third, the size of the field-cooled domains decreases with increasing fields. Villain predicted that the minimum metastable domain size would scale with field as $\kappa\sim H^{\nu_H}$ with $\nu_H=2$ at low temperatures.[39] From x-ray scattering data at fields below 3 T, we estimate $\nu_H=1.9\pm0.3$ for $Mn_{0.45}Zn_{0.55}F_2$ and $\nu_H=1.7\pm0.4$ for $Fe_{0.5}Zn_{0.5}F_2$; as noted previously, they are both consistent with the predicted $H^2$ behavior. However, the accuracies of these x-ray estimates are compromised by the fact that the data analysis only involved convolution in the transverse direction. We note that Hill *et al.* also found their FC x-ray data on $Mn_{0.75}Zn_{0.25}F_2$ to be compatible with $\nu_H=2.0$.[12]

That the appearance of the FC LRO might reflect the equilibrium random-field transition was first suggested by Hill *et al.*[12] Our result on $Fe_{0.5}Zn_{0.5}F_2$ rules out the possibility that the presence of the FC LRO in the earlier data is in some way due to the weak anisotropy of the $MnF_2$ system. The interpretation of an underlying equilibrium transition is further corroborated by our current neutron results which lend credence to the existence of such a transition below $T_M$, though we have not obtained accurate predictions for $T_N(H)$ at the lower fields directly from neutron scattering. Upon field heating, the observed LRO does not retrace the temperature dependence of the FC LRO, indicating that the FC LRO is not in equilibrium in the usual sense. As found in $Mn_{0.75}Zn_{0.25}F_2$, the exponent $\beta_{FC}$ is close to the random exchange Ising value, which perhaps suggests that the behavior at this presumed equilibrium random-field transition is somehow controlled by random exchange Ising criticality. At higher fields, the LRO never develops and only SRO is observed during FC. One important observation is that both the neutron and the x-ray results indicate the trend of increasing $[T_M(H)-T_N(H)]$ with increasing applied field, demonstrating that these are effects attributable to the random fields.

There remains the question regarding the origin of the field-cooled long range order. Two possible scenarios have been suggested. The first is that the LRO observed with x rays in fact coexists with the SRO throughout the bulk of the sample. The FC LRO is unexpected largely because it has never been seen in a neutron scattering experiment. However, at the low fields discussed here, the inverse domain size $\kappa$ is generally smaller than the broad neutron resolution and extinction effects are strong. To account correctly for extinction is quite difficult.[5] Further, the LRO intensity can be quite small and overshadowed by the strong SRO intensity as seen by neutrons. Thus it is not entirely impossible that this two length scale state was simply not observable in the neutron scattering data and analysis. While it seems unlikely that this is the case, in particular in light of the sensitivity of the FC LRO to surface treatment, neutron scattering with high resolution and adequate extinction correction may be necessary to settle this uncertainty.

A second scenario for the origin of the FC LRO, first proposed by Hill *et al.*,[12] is that the LRO results from defects in the near surface region of the samples. These defects may play a role in aiding the formation of LRO by, for example, providing nucleation centers for large magnetic clusters or generating an asymmetric distribution of random fields near the surface. This latter suggestion was stimulated by the work of Maritan *et al.*[40] who predicted that, in the case of asymmetric random fields, the observed value of $\beta$ should be that of the pure Ising model, 0.325, or in our case the random exchange Ising model, 0.35, and not the RFIM. The $\beta_{FC}$ estimated above is in agreement with this prediction and is consistently higher than $\beta_{ZFC}$ and $\beta_{FH}$. An additional observation that may shed some light on the origin of the LRO component is the subtly different longitudinal position of the LRO piece from the center of the SRO peak in the longitudinal scans. Note that the longitudinal direction is perpendicular to the crystal surface. This may indicate two different underlying lattice constants for the two different length scales—a situation that could conceivably occur because of a concentration of defects near the surface. However, this shift in the longitudinal peak position was not reported for $Mn_{0.75}Zn_{0.25}F_2$. Furthermore, the ZFC longitudinal scans are all resolution limited and do not seem to suffer from two offset components.

## VI. SUMMARY

In summary, we have studied the field-cooled transition of the 3D RFIM with neutron and x-ray magnetic scattering. Double-axis neutron scattering measurements of $Fe_{0.5}Zn_{0.5}F_2$ yield $\nu=1.5\pm0.3$, $\gamma=2.6\pm0.5$, and $\overline{\gamma}=5.7\pm1$ for the random-field correlation length, connected and disconnected susceptibility exponents, respectively. All of the analysis was carried out in the equilibrium regime, that is above the metastability temperature and below the zero field Néel temperature, where RFIM critical behavior is expected to be observed. The equilibrium random-field transition temperature is a fitting parameter in the power law fits to $\kappa$. The $T_N(H)$ determined in this way is well below $T_M(H)$ and $T_C(H)$, both determined from the ZFC transition data at the corresponding fields. Clearly, in order to determine the critical exponents more accurately, experiments need to go to higher fields where the random-field behavior may be observed over a wider accessible temperature range. Alternatively, one could take detailed measurements on approaching the transition at fixed temperature, by varying the external field.

The field-cooled x-ray data from $Fe_{0.5}Zn_{0.5}F_2$ and $Mn_{0.45}Zn_{0.55}F_2$ reveal the coexistence of long range order and short range order for weak random-field strengths. The nucleation of the long range order occurs below $T_M(H)$ and $T_C(H)$. The intensity of the long range order component decreases with increasing field. The LRO temperature dependence can be described by a power law with $\beta_{FC}\approx0.3\pm0.05$. The origin of this field-cooled long range order is not understood. To address these questions further, a high resolution neutron scattering study together with reliable extinction corrections is perhaps the most viable approach.

## ACKNOWLEDGMENTS

We would like to thank A. Aharony for valuable discussions of this work. The work at MIT was supported by the National Science Foundation under Grant No. DMR-9315715, and in part by the MRSEC Program of the National Science Foundation under Award No. DMR-9400334. The work at Brookhaven National Laboratory was carried out under Contract No. DE-AC02-76CH00016, Division of Materials Science, U.S. Department of Energy.

[1] T. Nattermann and J. Villain, Phase Transit. **11**, 5 (1988).
[2] Y. Imry and S. Ma, Phys. Rev. Lett. **35**, 1399 (1975).
[3] J. Z. Imbrie, Phys. Rev. Lett. **53**, 1747 (1984).
[4] S. Fishman and A. Aharony, J. Phys. C **12**, L729 (1979).
[5] R. A. Cowley, H. Yoshizawa, G. Shirane, and R. J. Birgeneau, Z. Phys. B **58**, 15 (1984).
[6] R. A. Cowley, G. Shirane, H. Yoshizawa, Y. Uemura, and R. J. Birgeneau, Z. Phys. B **75**, 303 (1989).
[7] D. P. Belanger, A. R. King, and V. Jaccarino, Phys. Rev. B **31**, 4538 (1985).
[8] D. P. Belanger, S. M. Rezende, A. R. King, and V. Jaccarino, J. Appl. Phys. **57**, 3294 (1985).
[9] R. J. Birgeneau, R. A. Cowley, G. Shirane, and H. Yoshizawa, Phys. Rev. Lett. **54**, 2147 (1985).
[10] P. Wong and J. Cable, Phys. Rev. B **28**, 5361 (1983).
[11] H. Yoshizawa, R. A. Cowley, G. Shirane, and R. J. Birgeneau, Phys. Rev. B **31**, 4548 (1985).
[12] J. P. Hill, Q. Feng, R. J. Birgeneau, and T. R. Thurston, Z. Phys. B **92**, 285 (1993).
[13] M. Lederman, J. V. Selinger, R. Bruinsma, J. Hammann, and R. Orbach, Phys. Rev. Lett. **68**, 2086 (1992).
[14] M. Lederman, J. V. Selinger, R. Bruinsma, R. Orbach, and J. Hammann, Phys. Rev. B **48**, 3810 (1993).
[15] P. Pollak, W. Kleenman, and D. P. Belanger, Phys. Rev. B **38**, 4773 (1988).
[16] I. B. Ferreira, A. R. King, and V. Jaccarino, Phys. Rev. B **43**, 10 797 (1991).
[17] Y. Shapira, N. F. Oliveira, Jr., and S. Foner, Phys. Rev. B **30**, 6639 (1984).
[18] E. T. Gawlinski, K. Kaski, Martin Grant, and J. D. Gunton, Phys. Rev. Lett. **53**, 2266 (1984).
[19] G. S. Grest, C. M. Soukoulis, and K. Levin, Phys. Rev. B **33**, 7659 (1986).
[20] Y. Kim and A. B. Harris, Phys. Rev. B **32**, 4676 (1985).
[21] U. Nowak and K. D. Usadel, Phys. Rev. B **46**, 8329 (1992).
[22] H. Yoshizawa and D. Belanger, Phys. Rev. B **30**, 5220 (1984).
[23] J. P. Hill, Q. Feng, Q. J. Harris, R. J. Birgeneau, A. P. Ramirez, and A. Cassanho, preceding paper, Phys. Rev. B **55**, 356 (1997).
[24] J. Villain, J. Phys. (France) **46**, 1843 (1985).
[25] D. Fisher, Phys. Rev. Lett. **56**, 416 (1986).
[26] R. J. Birgeneau, Q. Feng, Q. J. Harris, J. P. Hill, A. P. Ramirez, and T. R. Thurston, Phys. Rev. Lett. **75**, 1198 (1995).
[27] Q. Feng, R. J. Birgeneau, and J. P. Hill, Phys. Rev. B **74**, 3840 (1995).
[28] U. A. Leitão, W. Kleemann, and I. B. Ferreira, Phys. Rev. B **38**, 4765 (1988).
[29] J. P. Hill, T. R. Thurston, M. J. Ramstad, R. W. Erwin, and R. J. Birgeneau, Phys. Rev. Lett. **66**, 3281 (1991).
[30] Q. Feng, Ph.D. thesis, M.I.T., Cambridge, MA, 1996.
[31] R. A. Cowley, H. Yoshizawa, G. Shirane, M. Hagen, and R. J. Birgeneau, Phys. Rev. B **30**, 6650 (1984).
[32] P. W. Mitchell, R. A. Cowley, H. Yoshizawa, P. Böni, Y. J. Uemura, and R. J. Birgeneau, Phys. Rev. B **34**, 4719 (1986).
[33] M. Schwartz, J. Phys. C **21**, 753 (1988).
[34] H. Rieger, Phys. Rev. B **52**, 6659 (1995).
[35] M. Gofman, J. Adler, A. Aharony, A. B. Harris, and M. Schwartz, Phys. Rev. Lett. **71**, 1569 (1993).
[36] H. Rieger and A. P. Young, J. Phys. A **26**, 5279 (1993).
[37] A. Bruce and D. Wallace, J. Phys. A **16**, 1721 (1983).
[38] A. Ogielski and D. Huse, Phys. Rev. Lett. **56**, 1298 (1986).
[39] J. Villain, Phys. Rev. Lett. **52**, 1543 (1984).
[40] A. Maritan, M. R. Swift, M. Cieplak, M. H. W. Chan, M. W. Cole, and J. Bannavar, Phys. Rev. Lett. **67**, 1821 (1991).